

The summertime annular mode in the Northern Hemisphere and its linkage to the winter mode

Masayo Ogi¹

Frontier Research Center for Global Change, Japan Agency for Marine-Earth Science and Technology, Yokohama, Japan

Koji Yamazaki

Graduate School of Environmental Earth Science, Hokkaido University, Sapporo, Japan

Yoshihiro Tachibana²

Liberal Arts Education Center, Tokai University, Hiratsuka, Japan

Received 6 January 2004; revised 12 July 2004; accepted 12 August 2004; published 28 October 2004.

[1] The seasonal variations of the Northern Hemisphere annular mode (NAM) are investigated through empirical orthogonal function analysis of the zonally averaged geopotential height fields for each individual calendar month. Patterns of the winter and summer NAMs differ not only in the geopotential height fields but also in the mean meridional circulation and eddy structure. The summer NAM has a smaller meridional scale and is displaced poleward as compared to the winter NAM. The antinode on the lower-latitude side in the summer NAM is at the nodal latitude of the winter NAM. The summer NAM is more strongly related to surface air temperatures over Eurasia than the original Arctic Oscillation. The summer NAM is a wave-driven internal atmospheric mode that is maintained by both stationary and transient waves. The summer NAM is associated with the Arctic front, polar jet, and storm track around the Arctic Ocean. The winter-to-summer linkage described by M. Ogi et al. can be interpreted as a preferred transition from one polarity of the winter annular mode to the same polarity of the summer annular mode. The spring cryosphere, i.e., snow in Eurasia and sea ice in the Barents Sea, plays a supporting role in this transition. *INDEX TERMS*: 1620 Global Change: Climate dynamics (3309); 3309 Meteorology and Atmospheric Dynamics: Climatology (1620); 3319 Meteorology and Atmospheric Dynamics: General circulation; 3349 Meteorology and Atmospheric Dynamics: Polar meteorology; *KEYWORDS*: Northern Hemisphere's annular mode, Arctic Oscillation, winter-to-summer link

Citation: Ogi, M., K. Yamazaki, and Y. Tachibana (2004), The summertime annular mode in the Northern Hemisphere and its linkage to the winter mode, *J. Geophys. Res.*, 109, D20114, doi:10.1029/2004JD004514.

1. Introduction

[2] The Arctic Oscillation (AO) is the leading mode in empirical orthogonal function (EOF) analysis of wintertime monthly mean sea level pressure (SLP) anomalies and is characterized by a seesaw of atmospheric mass between middle and high latitudes. The AO is a notable atmospheric phenomenon over the Northern Hemisphere in winter [Thompson and Wallace, 1998] (hereinafter referred to as TW1998) and is characterized by a deep barotropic annular structure. Thompson and Wallace [2000] (hereinafter referred to as TW2000) used a single EOF analysis of the zonal mean geopotential height fields for all calendar months and showed that the AO dominates throughout the

year. The AO is also referred to as the Northern Hemisphere annular mode (NAM). Zonally symmetric flow anomalies associated with the winter NAM are forced by eddy momentum fluxes associated with stationary and transient waves [Limpasuvan and Hartmann, 1999, 2000]. TW2000 used regressions of circulation anomalies upon the standardized leading principal component (PC) time series of the spatially fixed leading EOF mode, which are constant with season, to study seasonal variations in the NAM. TW2000 revealed a winter-dominant mode, however, because atmospheric variability is largest in winter. There is no guarantee that the summer-dominant mode is the same as the winter mode extracted in TW2000. Thus the EOF analysis in TW2000 may not correctly extract the summer dominant mode. In this study, the seasonal variation of the AO/NAM is investigated more accurately through an application of an EOF analysis for each calendar month, individually.

[3] There are known links between the winter NAO/AO and summer climates. Ogi et al. [2003a, 2003b] showed that the extratropical Northern Hemisphere summertime climate is influenced by the NAO/AO of the previous winter,

¹Also at Graduate School of Environmental Earth Science, Hokkaido University, Sapporo, Japan.

²Also at Institute of Observational Research for Global Change, Japan Agency for Marine-Earth Science and Technology, Yokohama, Japan.

particularly during years of solar maxima. The summertime NAO/AO signal is annular, but its meridional extent is much smaller than in winter. The summertime atmospheric pattern hints at the link between the winter and summer NAM patterns. If the summer annular pattern is the dominant summer mode, the meridional scale of the summer NAM is smaller than that of winter. The summer pattern shown by *Ogi et al.* [2003a, 2003b] has not been shown to be the leading mode of the summertime atmospheric variation, although the pattern shown is likely to be the summertime NAM.

[4] Influenced by the above motivations, this study investigates the seasonal variation of the Northern Hemisphere annular mode, focusing in particular on the summer mode, and comparing the summer mode to the winter annular mode. In addition, the EOF analysis in this study is compared to the EOF analysis in TW2000. Relationships between the winter AO/NAM and subsequent summer circulation identified by *Ogi et al.* [2003a, 2003b] are interpreted from the viewpoint of a transition between the winter and summer annular modes.

2. Data and EOF Analysis

[5] Data to compute the modes originate from the NCEP/NCAR reanalysis data set for 1958 to 2002 [*Kalnay et al.*, 1996; *Kistler et al.*, 2001]. Monthly mean data are used in most of the analyses but daily data are used in calculations of eddy momentum flux and storm track. The AO index from 1958 to 2001 is from TW2000. An EOF analysis of the temporal covariance matrix is performed separately for each individual calendar month using monthly and zonally averaged geopotential height fields poleward of 40°N from 1000 hPa to 200 hPa. The EOF analysis yields seasonal variations in the primary mode of interannual variability in the northern extratropical troposphere. Data are weighted in the EOF analysis by the square root of the cosine of latitude and the square root of the pressure interval to ensure equal area and mass weighted contributions to the variance. The leading mode has a dipole structure between the Arctic and midlatitudes during all months. Variance explained by the first mode exceeds 50% in winter months and 35–50% in summer months. If the chosen domain is poleward of 20°N, as in TW2000, the summer leading mode has a uniform sign over the domain, but the second mode has a dipole pattern that is essentially the same pattern as the leading mode for the domain poleward of 40°N. A dipole pattern also emerges as the first mode for a domain poleward of 20°N if the EOF analysis is applied to zonal mean 1000-hPa geopotential heights.

[6] Horizontal sea level pressure (SLP) fields were also used in an EOF analysis of regions poleward of 40°N for individual calendar months. A seesaw between the Arctic and midlatitudes characterizes the leading mode (EOF1) in both summer and winter; the pattern is similar to that derived from the EOF of the zonal mean field. Indeed, the correlation coefficient between the score of the SLP-EOF1 and the zonal mean EOF1 for summer (June–August) is 0.86, which suggests that the two modes are essentially the same. An analysis using geopotential heights at 500 hPa (Z500) yielded similar results. The NAM dominates high-latitude variability patterns even in summer. However, the

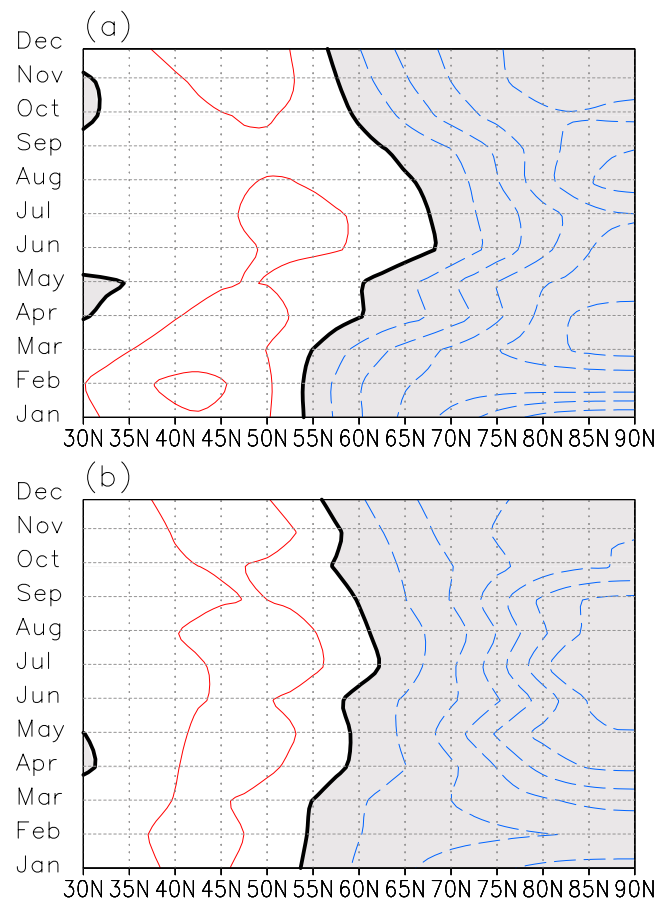


Figure 1. (a) Regression coefficients of monthly averaged zonal mean geopotential height at 500 hPa regressed against standardized PC time series of the leading EOF of the zonal mean geopotential height field for each month in the Northern Hemisphere. Shading denotes negative values. Solid red contours denote positive values, and dashed blue contours denote negative values. The zero contour is thick black. Contour interval is 10 m. (b) As in Figure 1a except for the AO index by *Thompson and Wallace* [2000].

leading mode of the SLP (Z500) fields in November (and October) does not show an annular pattern. Therefore the zonal mean geopotential height is adopted in order to define the annular mode in the present study.

3. Difference Between Winter and Summer NAMs

[7] The meridional structure of the NAM varies with season. Figure 1a shows the seasonal variation of the NAM as determined by a regression of the zonal mean 500-hPa geopotential height anomalies upon the standardized PC time series. From January to March, an oscillation between middle and high latitudes characterizes the leading EOF; the node is near 55°N, which agrees with the original AO. The seesaw pattern moves toward higher latitudes in April. The pattern is displaced farthest poleward in summer (June–July (JJ)), with the node near 65°N. The lower-latitude antinode in summer is near 50°N, near the winter nodal latitude. A slow southward shift of the node occurs

Table 1. Correlation Coefficients Between the SV NAM Index and the AO Index for 1958–2001

	Correlation Coefficient
January	0.92
February	0.93
March	0.94
April	0.88
May	0.89
June	0.70
July	0.72
August	0.84
September	0.82
October	0.72
November	0.84
December	0.93

from August to November. In December, the node returns to its winter position. A similar EOF analysis was performed for the Southern Hemisphere. As the meridional structure of the Southern hemisphere annular mode (SAM) did not vary with season, this paper will focus on the NAM. The standardized score of the principal component calculated from the projection of anomalies to the pattern of EOF1 for each month is hereafter called a seasonally varying NAM index (SV NAM index) simply to distinguish the index in the present study from the original AO/NAM index. SV NAM is not meant to imply that the winter and summer dominant variations belong to the same mode.

[8] The AO index (AOI) (TW2000), in contrast, shows less seasonal variability (Figure 1b). Table 1 shows the correlation coefficient between the SV NAM index and the AOI from TW2000 for each month in the 44 years from 1958 to 2001. Correlations are very high (exceeding 0.9) from December to March; in winter, the NAM in the present study is virtually identical to the AO. In June and July, however, the correlation coefficients between the SV NAM index and the AOI are 0.70 and 0.72. Patterns associated with the AOI in TW2000 vary little with season. Only a slight node shift is present in Figure 1b. Consequently, the summertime AOI does not reproduce the summer NAM pattern, which is consistent with the lower correlation between the SV NAM index and AOI during summer. To distinguish modes, the summer-dominant mode and the winter mode are hereafter called the summer NAM and the winter NAM, respectively. The antinode of the summer NAM is near the same latitude as the node of the AO; variances in the antinodal latitudes are not present at all in the AO. At polar latitudes, the amplitudes in both the AO and the summer NAM are large. Because the two patterns agree with each other only in the polar domain, it is reasonable that the correlation coefficient declines in summer. In the following analyses, “summer” is defined as June–July and “winter” as January–February, based on the timing of the extreme nodal positions.

[9] Figure 2 shows winter and summer geopotential height anomalies at 1000, 500 and 200 hPa as regressed on the SV NAM index. The winter surface pattern (Figure 2a, January–February mean) is characterized by a seesaw between middle and high latitudes, with a node near 55°N. The winter structure and amplitude agree with patterns in TW2000. Patterns at upper levels regressed onto the winter SV NAM index (Figures 2b and 2c) are similar to

the surface patterns (Figure 2a), reflecting the deep barotropic structure. The summer pattern is also characterized by a seesaw pattern at both surface (Figure 2d) and upper levels (Figures 2e and 2f), but the amplitude does not increase greatly with height and the signal is mainly confined to the troposphere. In addition, the area of negative anomalies in the Arctic is smaller in summer than in winter, and the zero anomaly line in summer is poleward of the winter zero anomaly line. Portions of central Eurasia extending from the Arctic have negative anomalies in winter and positive anomalies in summer. The poleward shift from winter to summer is particularly evident over eastern Eurasia, the Pacific and Canada. Furthermore, strong negative anomalies are seen over Greenland in winter. In summer, the negative anomalies are over the central Arctic Ocean. These features extend through the entire troposphere.

[10] Figure 3 shows zonal means of zonal wind anomalies (contours in Figures 3a and 3b), temperature anomalies (contours in Figures 3c and 3d) and meridional circulation anomalies (vectors in all panels) regressed onto the SV NAM index. Shading indicates correlation coefficients between the zonal mean zonal wind and the SV NAM index. A dipole structure of negative correlation in midlatitudes and positive correlation in high latitudes is present, both in winter and summer, from troposphere to stratosphere. However, the node of the zonal wind anomalies is at a higher latitude in summer (Figure 3b, near 50°N) than in winter (Figure 3a, near 40°N). In both summer and winter modes, high-latitude positive anomalies extend into the stratosphere. The summer high-latitude wind anomaly peaks at the tropopause. In winter, the anomaly extends into the stratosphere and peaks around 30 hPa.

[11] Figures 3c and 3d show zonal mean temperatures regressed onto the same indices. During both winter and summer, warm zonal mean temperature anomalies coincide with a node of the zonal wind anomalies, a relationship that is consistent with thermal wind. The warm summer temperature anomaly is displaced poleward relative to the winter anomalies. Cold anomalies in winter extend from the troposphere to the middle stratosphere. In contrast, cold anomalies in summer are restricted to the troposphere and warm anomalies occur above the tropopause, which is consistent with decaying geopotential height anomalies above the tropopause. TW2000 showed a similar figure (their Figure 9) for summer (June, July, and August) based on the AOI, which figure resembles Figure 3 in structure, but the magnitude of their results is smaller than in the present study.

[12] The associated meridional motions (arrows in Figure 3) describe an indirect circulation between middle and high latitudes. This circulation suggests that Coriolis acceleration maintains the surface wind anomalies against surface friction. In the upper troposphere, eddy momentum flux helps maintain the wind anomalies.

[13] Figure 4 shows the zonal mean poleward eddy momentum flux, $\overline{u'v'}$, regressed onto the SV NAM index. The primes in $u'v'$ denote deviation from the zonal mean, and the overbar denotes zonal average. The stationary eddy momentum flux is calculated from monthly mean data. The transient eddy momentum flux results from subtracting the stationary flux from the total eddy momentum flux.

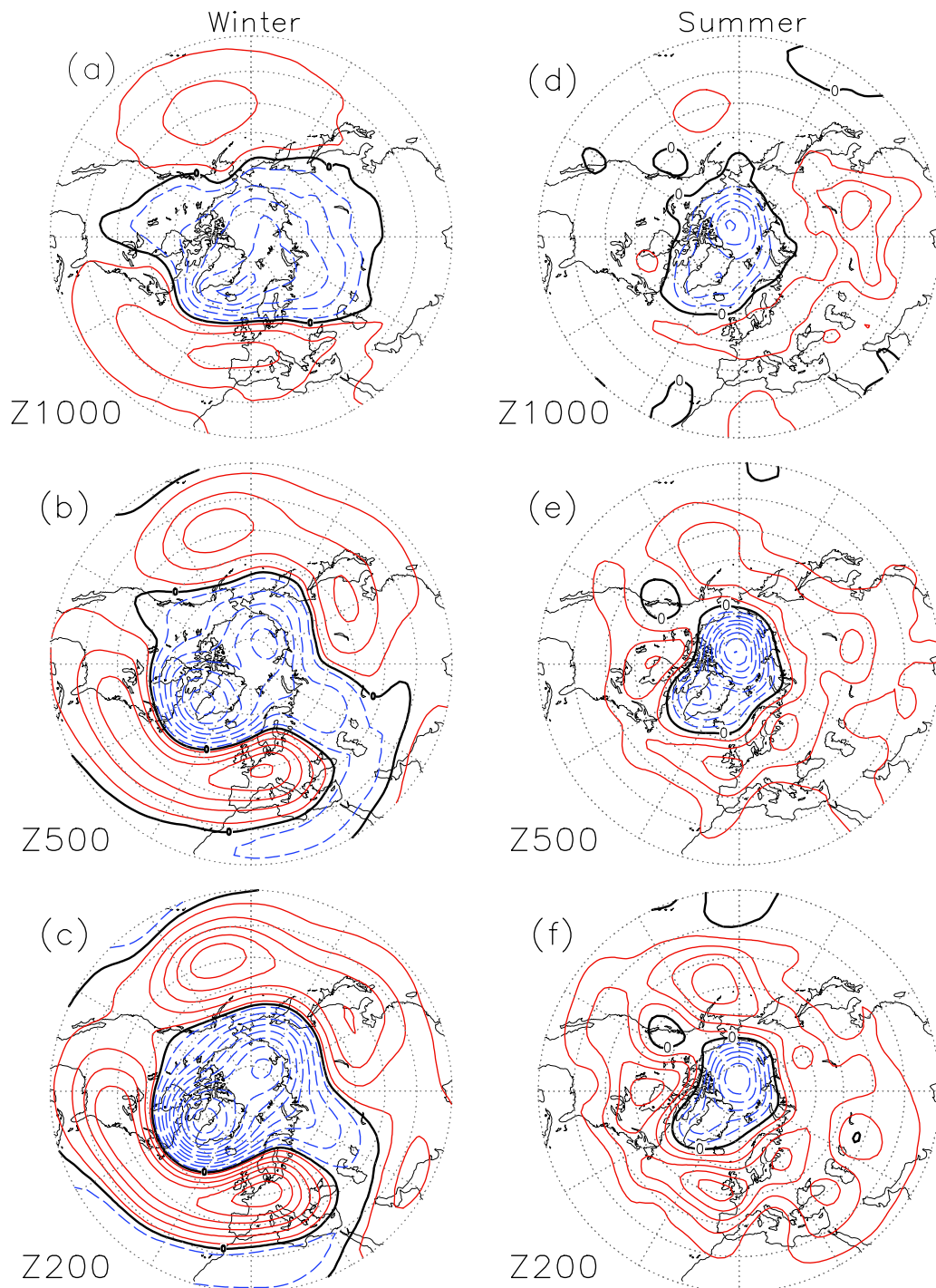


Figure 2. (a) Horizontal map of geopotential height at 1000 hPa regressed on the winter (January–February) SV NAM index. Red solid contours denote positive values, and blue dashed contours denote negative values. Contour interval is 10 m (e.g., -25 , -15 , -5 , 5 , 15 , ...). The zero contour is thick black. (b) As in Figure 2a but for 500 hPa. (c) As in Figure 2a but for 200 hPa. (d, e, and f) As in Figures 2a, 2b, and 2c but for summer (June–July). The contour interval is 5 m (e.g., -15 , -10 , -5 , 5 , 10 , ...).

Total flux is calculated from daily data. The strongest anomalies of the total eddy flux (Figures 4a and 4d) are near 45° – 60° N at 300-hPa in winter and near 50° – 65° N at 300-hPa in summer. Total eddy flux in winter is attributed mainly to stationary waves (Figure 4b); transient eddies (Figure 4c) are weak. However, both stationary and tran-

sient eddies (Figures 4e and 4f) help maintain the summer NAM.

[14] Figure 5 shows the eddy forcing at 300-hPa, the level at which eddies are strongest. The strongest eddy forcing during winter (Figure 5a) is near 60° N and stationary wave forcing dominates contributions by transient waves.

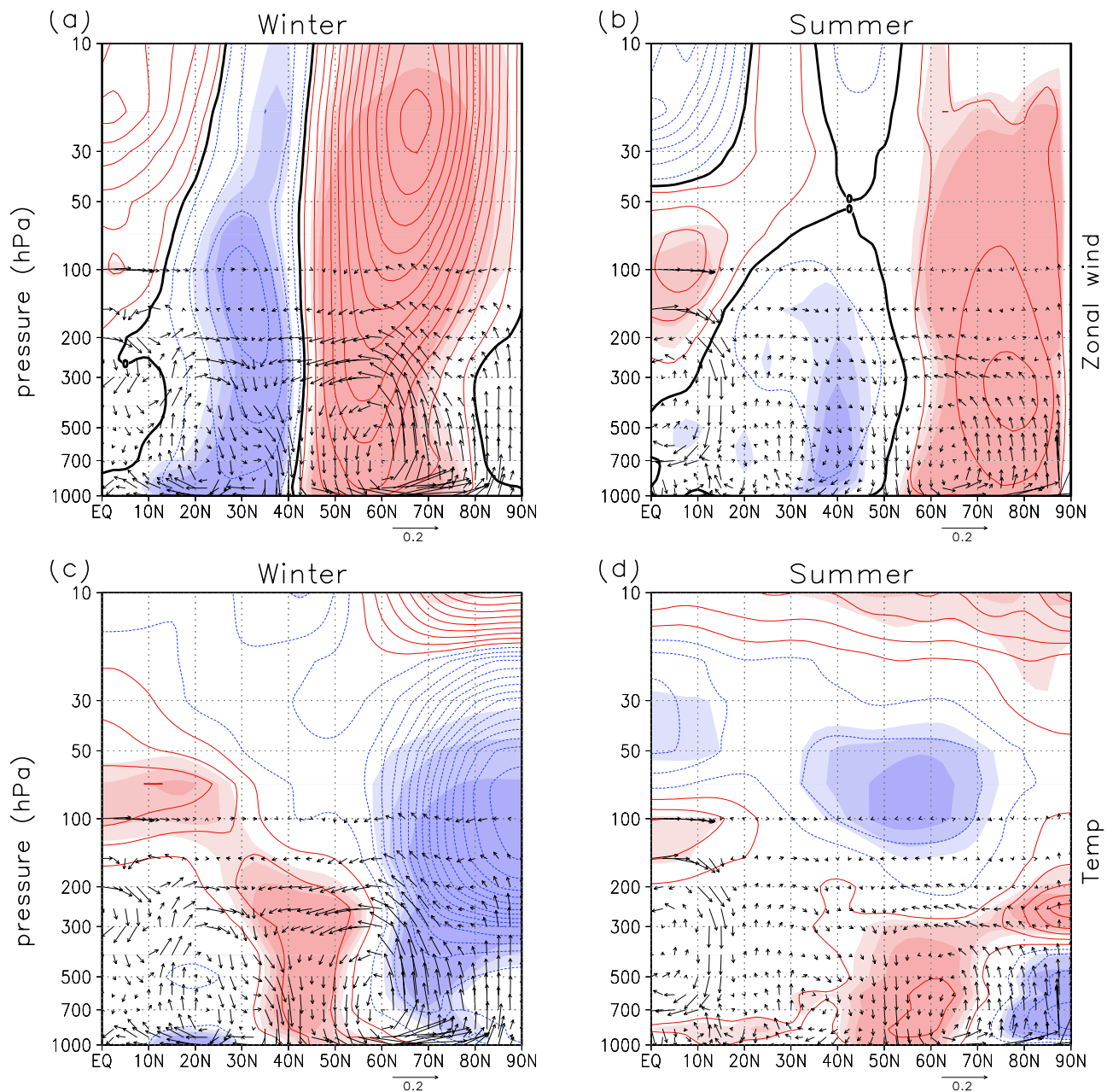


Figure 3. Latitude-height cross sections of the zonal mean zonal wind (contours, contour interval of 0.5 m/s, i.e., $-1.25, -0.75, -0.25, 0.25, \dots$) and zonal mean meridional circulation (vectors) regressed on the (a) winter and (b) summer NAM index. Light, medium, and heavy shading indicates correlation coefficients that exceed the 95, 99, and 99.9% confidence levels, respectively. Vectors above 100 hPa are not drawn where vertical velocity is unavailable. (c and d) As in Figures 3a and 3b but for contours of zonal mean temperature. Contour interval is 0.2 K (e.g., $-0.5, -0.3, -0.1, 0.1, 0.3, \dots$). Zero contours are drawn by thick black line in Figures 3a and 3b.

In contrast, the strongest eddy forcing during summer (Figure 5b) is near 70°N, which is poleward of the strongest winter forcing. In addition, the stationary and transient components of eddy forcing are of comparable size.

[15] Eddy heat flux indirectly affects the zonal mean wind. It is therefore appropriate to examine the eddy heat flux associated with the NAMs. In winter, eddy heat flux in the lower troposphere is enhanced at high latitudes, and reduced at mid latitudes, in association with a positive SV

NAM index. The correlation is small in summer, however (not shown), because eddies associated with the summer NAM are nearly barotropic.

4. Westerly Jets and Storm Tracks Associated With the Winter and Summer NAMs

[16] The previous section showed that eddy forcing maintains the zonal mean zonal winds of both winter and

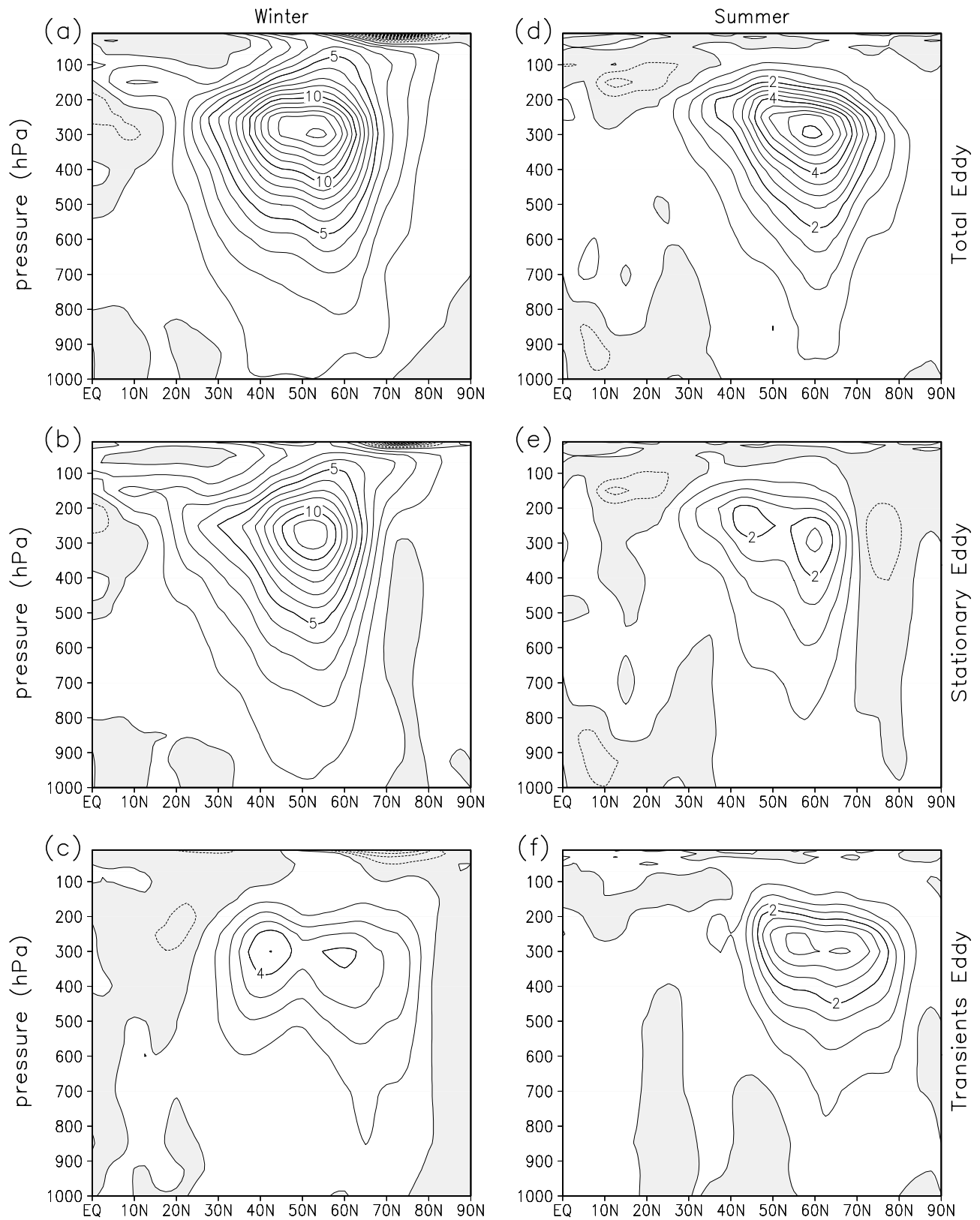


Figure 4. (a, b, and c) Winter and (d, e, and f) summer poleward eddy momentum flux regressed on the SV NAM index. (top) Total eddy momentum flux. (middle) Stationary eddy momentum flux. (bottom) Transient eddy momentum flux. See text for details. The contour interval is 1 m²/s² in winter, 0.5 m²/s² in summer; negative values are shaded.

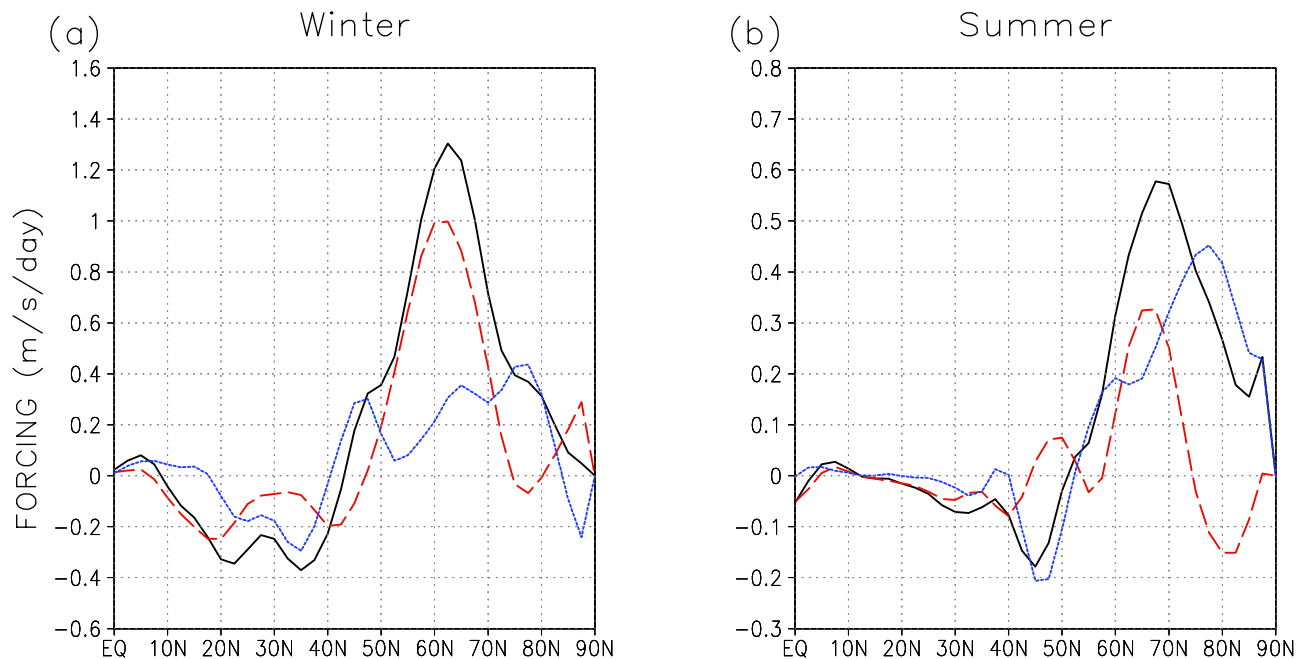


Figure 5. (a) Winter and (b) summer wave forcing profiles at 300 hPa owing to eddy momentum flux regressed on the SV NAM index. The solid line denotes the total wave forcing, the dashed red line denotes stationary wave forcing, and the dotted blue line denotes transient wave forcing.

summer NAMs. In this section, horizontal patterns of lower tropospheric temperature, upper tropospheric jets, and transient wave activity associated with NAMs are discussed.

[17] Figures 6a and 6b show 850-hPa temperatures and the magnitude of the temperature gradient in years of extreme positive (+3) and negative (−3) summer NAM indices, respectively. Large temperature gradients surround the Arctic Ocean during positive summer NAM years (Figure 6a). This enhanced thermal contrast indicates the enhanced baroclinicity that enhanced the transient eddy activity along the coastline in the positive summer NAM years shown in Figures 4f and 5b. In particular, the Arctic frontal zone [Serreze *et al.*, 2001] is active during positive summer NAM years. For the negative summer NAM years (Figure 6b), in contrast, the Arctic frontal zone is obscure.

[18] The thermal wind relationship suggests strong westerly winds should overlay the strong meridional temperature gradients. Figures 7a and 7b show the climatology of the 300-hPa zonal wind in Northern Hemisphere winter (January–February) and summer (June–July). Strong jets over the western Pacific and over the western Atlantic are present in winter (Figure 7a). The summer jet at 300 hPa (Figure 7b) shifts toward higher latitudes and has a more annular shape than in winter. Over Eurasia, the jet is located north of the Tibetan Plateau in summer. No distinct jet exists over northern Siberia in the summer climatology. Zonal winds at 300 hPa regressed onto the winter NAM (Figure 7c) show a northeastward shift of the jet stream. The summer 300-hPa zonal wind anomaly regressed onto the summer NAM (Figure 7d) reveals a zonal pattern around the Arctic Ocean that indicates the enhancement of the polar jet.

[19] Figures 7e and 7f show the winter and summer 300-hPa zonal wind when the SV NAM index is +3. Zonal wind values are obtained by summing the mean and three times the regression coefficient. The winter jet stream (Figure 7e) is strong and extends to northern Europe. On the other hand, the summer jet stream associated with the summer NAM (Figure 7f) is characterized by a strong westerly wind area surrounding the Arctic Ocean, and a double jet structure appears over Eurasia, the Pacific Ocean and North America. Serreze *et al.* [2001] noted that the heat contrast between the Arctic Ocean and adjacent continents influences the upper tropospheric zonal wind and the eddy activity in the Arctic frontal zone. The present analyses show that the subpolar jet associated with the Arctic frontal zone is discernible only in the positive phase of SV NAM.

[20] Daily NCEP/NCAR reanalysis data of 300-hPa geopotential height variance reveal storm tracks related to eddy activity that is associated with the winter and summer NAMs. Geopotential height variance is high-pass filtered using a Hamming window [Hamming, 1989] with $T = 7$ days that passes variability higher than 7 days and stops variability lower than 14 days. Storm tracks, regions of enhanced synoptic-scale transient eddies in the Northern Hemisphere winter, are located downstream of the westerly jet cores over the North Atlantic and the North Pacific [Blackmon *et al.*, 1977]. Regression of the winter storm track onto the winter NAM index reveals enhanced activity over the North Atlantic and North Pacific when the NAM has positive values (Figures 8c and 8e). Wintertime regression patterns over the North Atlantic agree with previous studies using the NAO index [e.g., Rogers, 1997; Hurrell and van Loon, 1997; Serreze *et al.*, 1997; Hurrell *et al.*, 2003].

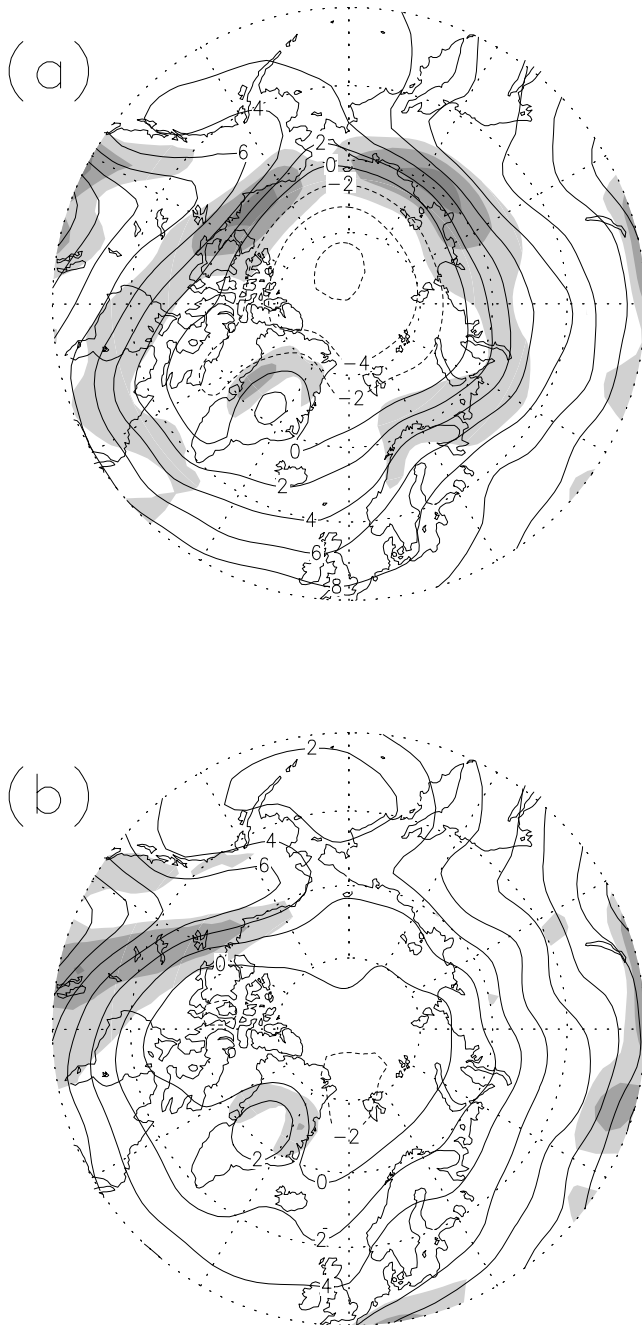


Figure 6. Summer 850-hPa temperature (contour) and the magnitude of the temperature gradient (shade). (a) Case in the SV NAM index for +3. (b) Same as in Figure 6a but for -3. Light and heavy shadings indicate values exceeding 6×10^{-3} K/km and 8×10^{-3} K/km, respectively.

[21] Storm tracks are also located over the North Atlantic and the North Pacific in summer. Storm intensities are reduced, and storm locations are poleward of winter storms (Figure 8b). A third storm track is along the Arctic coast of Eurasia, an extension of the Atlantic storm track. The North Atlantic and Arctic storm tracks are enhanced only when the summer NAM is positive, when a ring-shaped storm track forms around the Arctic Ocean in addition to the North Pacific storm track (Figures 8d and 8f). An Arctic storm

track is characteristic only of the summer positive NAM, and corroborates the differences between the summer NAM and the winter NAM (or the original AO/NAM). Both baroclinic waves and quasi-stationary Rossby waves contribute to the Arctic eddy activity. Strong westerlies along the Arctic coast of Eurasia act as a waveguide for Rossby waves, and wave trains are observed in the summer of positive NAM years [Ogi *et al.*, 2004]. These waves may maintain the double-jet structure through zonal-eddy coupling [Limpasuvan and Hartmann, 1999, 2000; Yamazaki and Shinya, 1999; Kimoto *et al.*, 2001], although there have been few studies for summer. Future studies will clarify the dynamic characteristics of the Arctic storm track and the double-jet structure.

5. Difference Between the Summer NAM and the Summer AO

[22] The present study has shown differences in structure and strength between the winter and summer dominant annular modes. This section discusses differences between the summer NAM in the present study and the summer AO in TW2000. The patterns of the summer 500-hPa geopotential height regressed onto the summer SV NAM index and the original AO index differ widely over Eurasia and Greenland (Figure 9). Figure 10 shows the summer surface air temperatures regressed onto the summer SV NAM index (Figure 10a) and the AO index (Figure 10b). The regression pattern of the summer SV NAM index shows positive values over Eurasia (Figure 10a). However, positive values are less notable over Eurasia in the AO case than in the summer NAM, especially over eastern Eurasia (Figure 10b).

6. Persistence and Seasonal Linkage of the Annular Modes

[23] Figure 11 shows lag regression/correlation coefficients between the zonal mean geopotential height at 500 hPa and the winter (JF) SV NAM index. In March, the correlation/regression patterns weaken. The positive correlations/regression values are significant from April to July around 50° – 65° N, latitudes that include the nodal latitudes of the winter seesaw pattern. The winter-to-summer linkage shown in Figure 11 is similar to Figure 1 of Ogi *et al.* [2003a], which used the NAO index as the winter index, because the AO/NAM and the NAO are highly correlated and are not separable in winter [e.g., Rogers and McHugh, 2002]. No correlation/regression coefficients appear after August; there are no significant connections from the previous winter to subsequent fall and winter.

[24] Figure 12 shows the horizontal structure of summertime 500-hPa geopotential height anomalies regressed upon the winter NAM index, confirming the winter-to-summer linkage. The pattern is characterized by a seesaw pattern with negative anomalies in the Arctic and positive anomalies in the subarctic. The pattern correlation between Figure 2b (the winter NAM) and Figure 12 poleward of 40° N is 0.22, indicating that the winter NAM does not simply persist until summer. In addition, the pattern linking winter to summer (Figure 12) is quite similar to the summer NAM pattern (Figure 2e). The pattern correlation

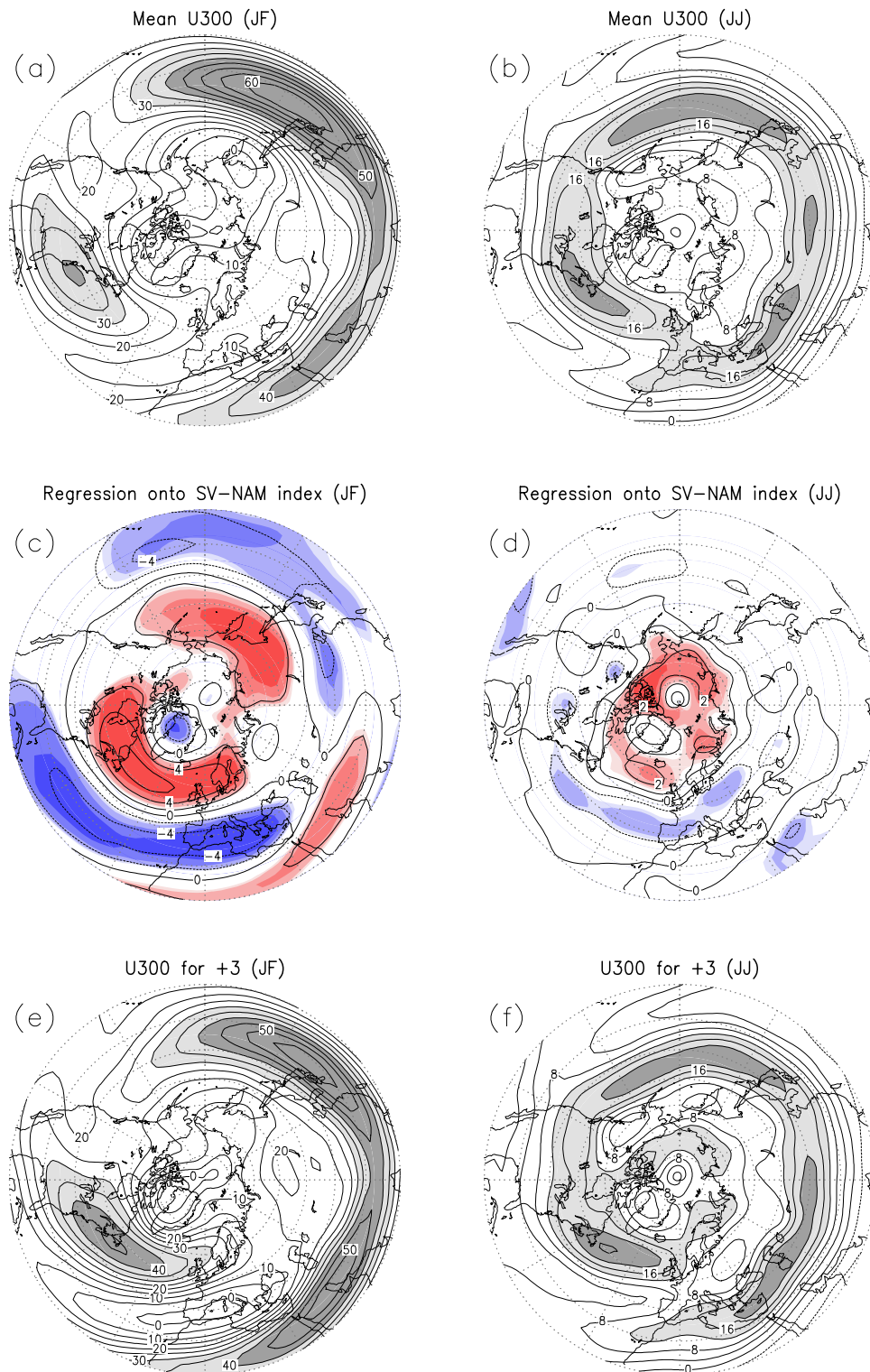


Figure 7. Zonal wind climatology at 300 hPa for (a) winter (January–February) and (b) summer (June–July) for 1958–2002. Contour intervals are 5 m/s (Figure 7a) and 4 m/s (Figure 7b). Light and heavy shadings denote values exceeding 30 m/s and 40 m/s (Figure 7a) and 12 m/s and 20 m/s (Figure 7b). Zonal wind field regressed onto the SV NAM index (contour) for (c) winter and (d) summer. Contour interval is 2 m/s (Figure 7c) and 1 m/s (Figure 7d). Light, medium, moderate, and heavy shadings indicate correlation coefficients that exceed the 90, 95, 99, and 99.9% confidence levels, respectively. Zonal wind fields when the SV NAM index is +3 for (e) winter and (f) summer. Contour interval and shadings in Figures 7e and 7f are the same as in Figures 7a and 7b, respectively.

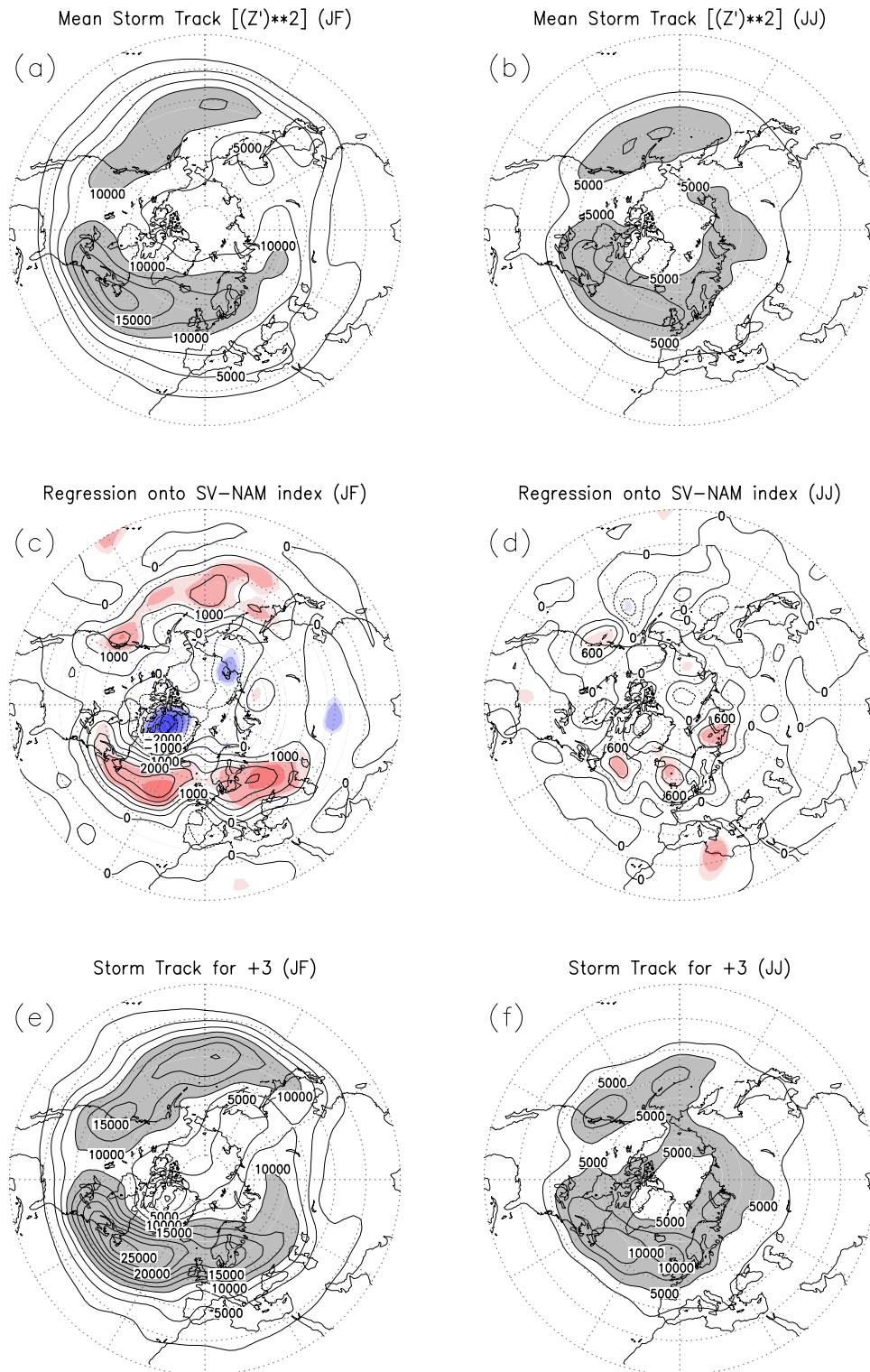


Figure 8. (a) Mean storm tracks for 1958–2002 winters (January–February) as revealed by the variance of the 300-hPa high-passed geopotential height. See text for details. (b) As in Figure 8a except for summer (June–July). The contour interval is 2500 m^2 . Shadings indicate values greater than 10,000 m^2 (Figure 8a) and 5000 m^2 (Figure 8b). (c) Storm track anomalies expressed in terms of amplitude by regression onto the winter SV NAM index. (d) As in Figure 8c, but for summer. Contour intervals are 500 m^2 (Figure 8c) and 300 m^2 (Figure 8d). Light, medium, moderate, and heavy shadings indicate correlation coefficients that exceed the 90, 95, 99, and 99.9% confidence levels, respectively. Storm tracks when the SV NAM index is +3 for (e) winter and (f) summer. Contour intervals and shadings in Figures 8e and 8f are as in Figures 8a and 8b, respectively.

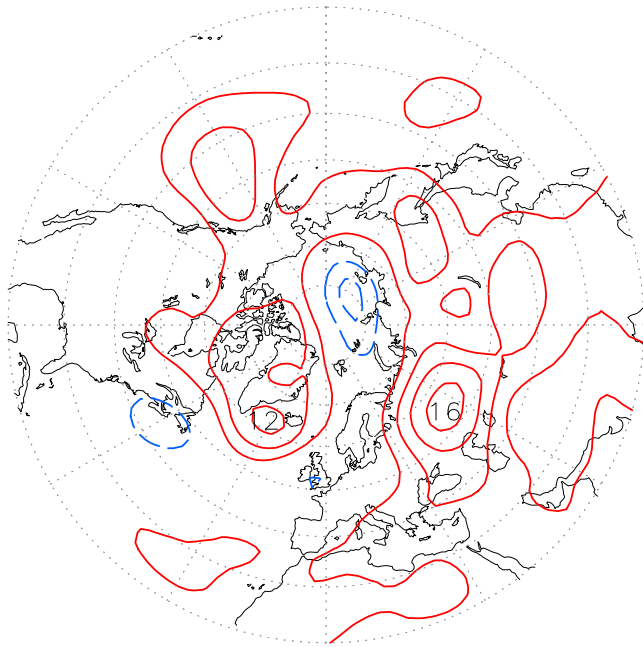


Figure 9. The difference between the summer (June–July) 500-hPa geopotential heights regressed onto the SV NAM index shown by the present study with those regressed onto the AO index shown by *Thompson and Wallace* [2000]. Red solid contours denote positive values, and blue dashed contours denote negative values. The contour interval is 4 m (e.g., $-8, -4, 4, \dots$). The zero contour is not drawn.

between Figures 2e and 12 over the domain north of 40°N is 0.75, and that for the area north of 50°N is 0.82.

[25] Lag correlation coefficients of the SV NAM index were calculated (Table 2) to further examine persistence

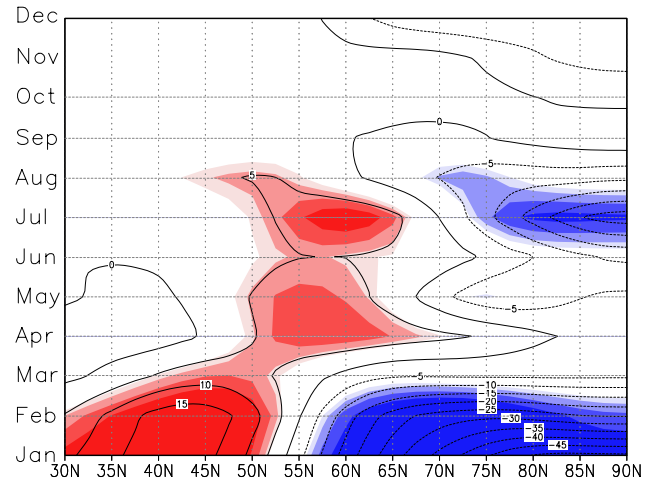
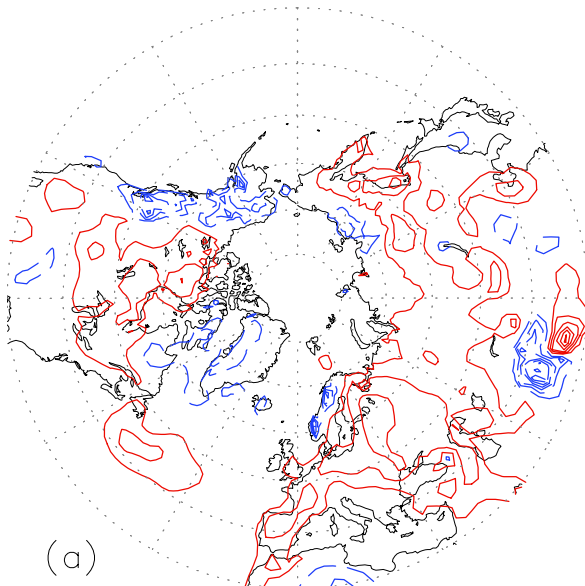


Figure 11. Lag regression coefficients between monthly averaged zonal mean 500-hPa geopotential height and the winter SV NAM index. Contour interval is 5 m. Shading indicates confidence levels (90, 95, 99, and 99.9%).

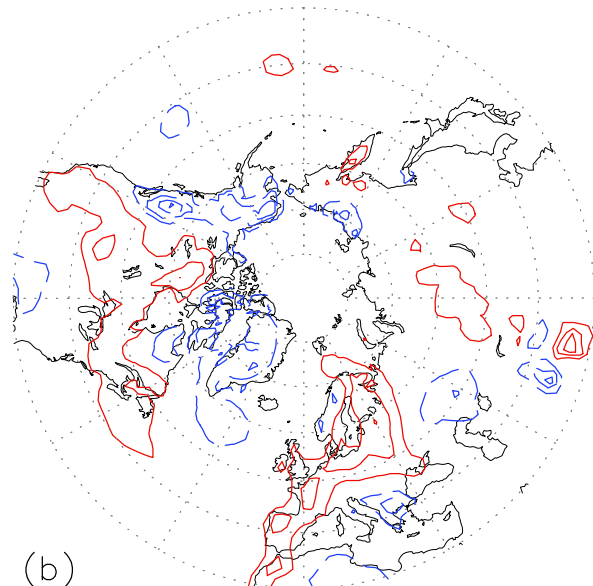
and seasonal linkage of the SV NAM. Persistence in spring and early fall is quite weak: a significant correlation at a 95% significance level is not present even between adjacent months. In contrast, adjacent months in winter and summer, such as January–February and June–July, have significant correlations at a 99% significance level. Furthermore, correlations between winter and subsequent summer months such as January–July and February–July also show significance at a 99% level. On the other hand, the summer-to-winter linkage is quite weak, weaker than the fall-to-winter linkage. The winter-to-summer linkage

SV–NAM index

AO index



(a)



(b)

Figure 10. (a) The summer (June–July) surface air temperature (2-m temperature) regressed on the SV NAM index. Solid red contours denote positive values; dashed blue contours denote negative values. Contour interval is 0.2 K (e.g., $-0.4, -0.2, 0.2, \dots$). The zero contour is not drawn. (b) As in Figure 10a except for the AO index by *Thompson and Wallace* [2000].

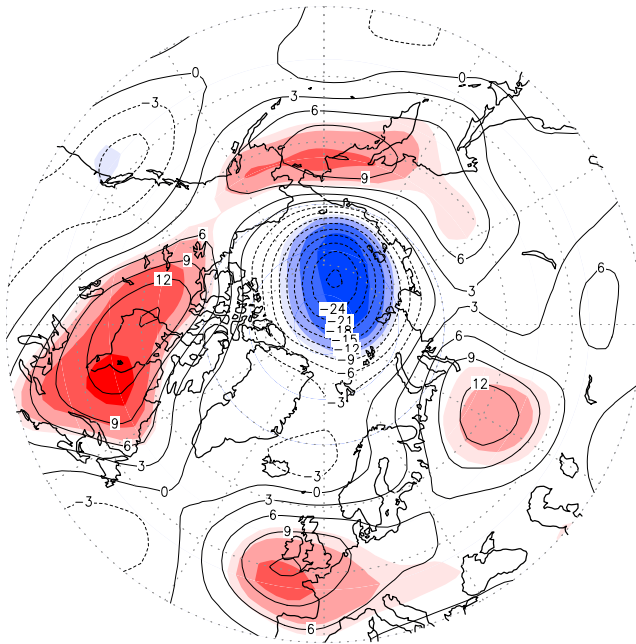


Figure 12. The summer (June–July) 500-hPa geopotential height regressed on the winter (January–February) SV NAM index. Contour interval is 3 m. Shading indicates confidence levels (90, 95, 99, and 99.9%).

is the preferred transition from the winter NAM to the summer NAM.

7. Solar Cycle Modulation of the Seasonal Linkage of the SV NAM

[26] This section investigates solar cycle modulation of the winter-to-summer atmospheric connectivity with the winter NAM. Kodera [2002, 2003] found that the structure of the winter NAO is modulated by the 11-year solar cycle. Ogi *et al.* [2003b] separated years according to the phase of the 11-year solar cycle, extending the analysis to the winter-to-summer linkage of the NAO and finding the strongest linkage during active solar years. In the present study, all years are separated into two phases of the solar cycle based on the winter solar activity data; solar

maxima (max) and solar minima (min), depending on whether the solar fluxes exceed or are less than a mean value. Winter solar activity is quantified by the winter (DJF) mean 10.7-cm solar radio flux data from 1957/58 to 2001.

[27] Figure 13 shows lag correlations of the monthly averaged zonal mean 500-hPa geopotential height with the winter NAM index for solar max and min years. During solar max years (Figure 13a), the winter correlation pattern is characterized by a seesaw between middle and high latitudes. The positive correlation pattern persists in mid latitudes through July, shifting poleward. During solar min years (Figure 13b), the winter correlation patterns are also characterized by a seesaw pattern. However, correlation patterns in spring and summer show no statistical significance. The correlation coefficient between the DJF mean winter NAM and the JJ mean summer NAM index for all 44 years is 0.31; it is statistically significant at a 95% confidence level. The corresponding correlation coefficient and significance level for the 20 solar max years is 0.52 and 98%. For the 24 solar min years, the correlation coefficient is 0.06 and it is not significant.

[28] Figure 14 shows horizontal patterns of 500-hPa geopotential height related to the winter NAM during solar max and solar min years. The correlation patterns show planetary-scale structures over midlatitudes and the Arctic in both solar max (Figure 14a) and solar min (Figure 14b) winters, although Arctic and Eurasian anomalies are larger during solar max years. During solar max years, spring is still characterized by a seesaw pattern, albeit with smaller correlations than in winter. In contrast, during solar min years, the seesaw pattern is not present. Summer signatures related to the winter NAM are characterized by a seesaw pattern only during solar max years (Figure 14e). The present spatial patterns are similar to the summer signal of the winter NAO of Ogi *et al.* [2003b] both for solar max and min years. The winter-to-summer linkage of the SV NAM is modulated by the 11-year solar cycle, as is the linkage of the NAO. Because the record covers only four solar cycles, however, further studies are needed to confirm the relationship.

[29] Ogi *et al.* [2003b] suggested that the signal of the winter NAO can be imprinted in the spring snow cover, sea ice, and surface oceans. Such a signal clearly exists only during solar max years. A similar analysis for SV NAM

Table 2. Lag Correlation Coefficients of the SV NAM Index

	Jan.	Feb.	March	April	May	June	July	Aug.	Sept.	Oct.	Nov.	Dec.	Jan.
Jan.		0.39 ^a											
Feb.			0.12										
March				−0.04	0.19	0.14	0.40 ^a	0.31 ^b	0.09	0.18	0.22	0.24	0.06
April					0.04	0.19	0.26	0.48 ^a	0.18	−0.10	−0.25	−0.16	0.14
May						0.15	0.05	−0.06	0.12	−0.02	0.13	0.29 ^b	0.13
June							0.08	−0.22	0.04	−0.09	0.13	−0.05	−0.03
July								0.25	0.01	−0.13	0.21	0.06	0.06
Aug.									0.51 ^a	0.34 ^b	0.15	−0.02	0.12
Sept.										0.36 ^b	0.14	−0.21	0.04
Oct.											0.07	0.08	0.09
Nov.												0.18	0.22
Dec.													0.00
Jan.													
Feb.													
March													
April													
May													
June													
July													
Aug.													
Sept.													
Oct.													
Nov.													
Dec.													

^aCorrelation coefficients exceed the 99% confidence levels.

^bCorrelation coefficients exceed the 95% confidence levels.

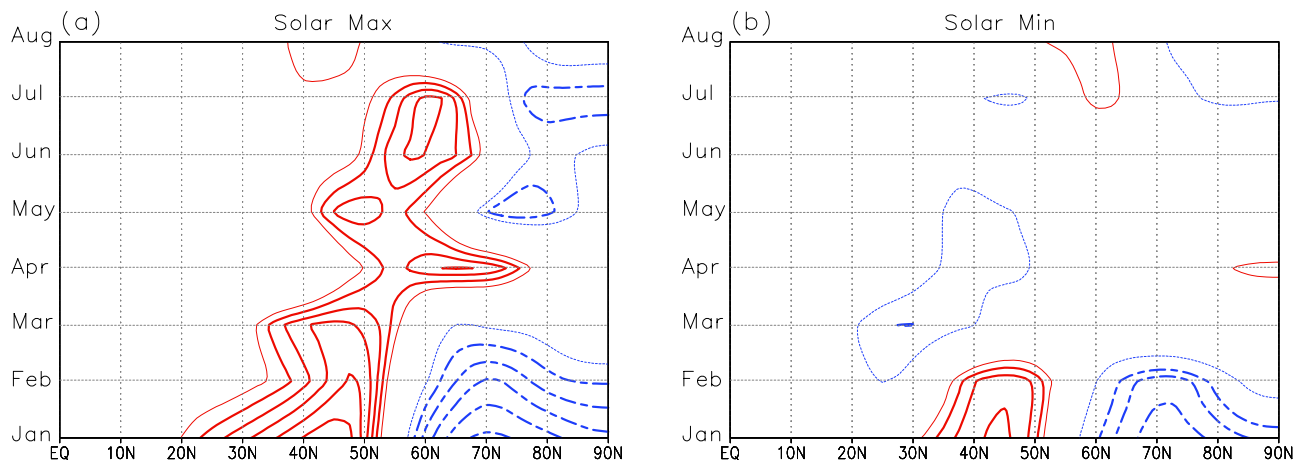


Figure 13. Lag correlation coefficients of monthly averaged zonal mean 500-hPa geopotential height with the winter (December–February) SV NAM index during the solar (a) maximum and (b) minimum phases. The contour interval is 0.1, and absolute values below 0.3 are omitted (thin lines are 0.3). Solid red contours denote positive values; dashed blue contours denote negative values.

yields results similar to Figure 5 of *Ogi et al.* [2003b] (not shown), reaffirming the key role of the surface cryosphere and SSTs in the winter-to-summer linkage.

8. Summary and Discussions

[30] Analyses in Section 3 revealed differences in winter and summer annular modes through application of an EOF analysis to each calendar month individually. The present EOF analysis has demonstrated that the NAM changes its structure with season, in contrast to the pattern simply projected by the conventional AO index shown by TW1998 and TW2000, which did not vary with season. The NAM in summer has a smaller meridional scale than the winter mode, and the center of action is over the Arctic Ocean in summer, and over Greenland in winter. Moreover, the characteristics of the summer annular mode are dissimilar to those of winter. The summer meridional circulation is shifted poleward by about 10° as compared to the winter circulation. Positive temperature anomalies coincide with the nodes of zonal wind anomalies. Thus the summer temperature anomaly is also shifted poleward relative to the winter temperature anomaly. Eddy momentum flux associated with the summer NAM also shifts poleward by about 10° as compared to the winter NAM. The wintertime NAM is a wave-driven internal atmospheric mode, and the forcing is maintained mainly by stationary waves [*Limpasuvan and Hartmann, 1999, 2000; Yamazaki and Shinya, 1999; Kimoto et al., 2001*]. Both stationary and transient waves maintain the summer NAM. During positive summer NAM years, the polar jet over the Arctic coasts of Eurasia and North America is manifest as a double-jet structure. A storm track along the polar jet over the coast of the Arctic Ocean is prominent. The present study has detailed the existence of the summer NAM, which differs from the winter NAM or the original AO/NAO. The summer NAM is more strongly related to surface air temperatures over Eurasia than is the conventional AO.

[31] Statistical methods have been used to derive the annular modes. These derived modes may or may not represent physical modes. Even for the original AO/NAM, there is debate on this issue [*Ambaum et al., 2001; Itoh, 2002; Wallace, 2000; Wallace and Thompson, 2002*]. Recently, S. Maeda (personal communication, 2004) calculated eigenmodes using the nondivergent barotropic vorticity equation and a 12-year mean field at 300 hPa and showed that one phase of the second unstable mode for the summer mean field in double-jet years resembles the summer NAM in the present study. This suggests that the summer NAM in the present study may have a physical basis. Further studies will clarify the dynamic characteristics of the summer NAM.

[32] The wintertime NAM/AO is linked to the summer atmospheric circulation. Summer atmospheric anomalies are similar to the summer NAM. The winter NAM and subsequent summer NAM have significant lagged correlations. The link between the winter NAM and the summer NAM can be interpreted as a preferred transition from one mode in winter to a similar mode in summer. For example, a winter circulation in a positive phase of the winter NAM is likely to be followed by a summer circulation in a positive phase of the summer NAM. Similarly, negative phase will likely follow negative phase. The continuation of the same phase in summer is possibly facilitated by springtime boundary conditions such as snow cover, as suggested by *Ogi et al.* [2003a, 2003b]. When the polarity of the winter NAO/AO is positive, spring-summer snow cover over the Arctic coasts of Eurasia and North America is reduced, which in turn enhances the meridional thermal contrast between the colder Arctic Ocean and the surrounding warmer continents. The larger thermal contrast could favor a positive polarity of the summer NAM by triggering enhanced eddy activity along the Arctic frontal zone [*Serreze et al., 2001*]. Further observational and modeling studies are required to support this hypothesis. The present study yields a basis for seasonal forecasts of the summer climate over the Northern Hemisphere extratropics.

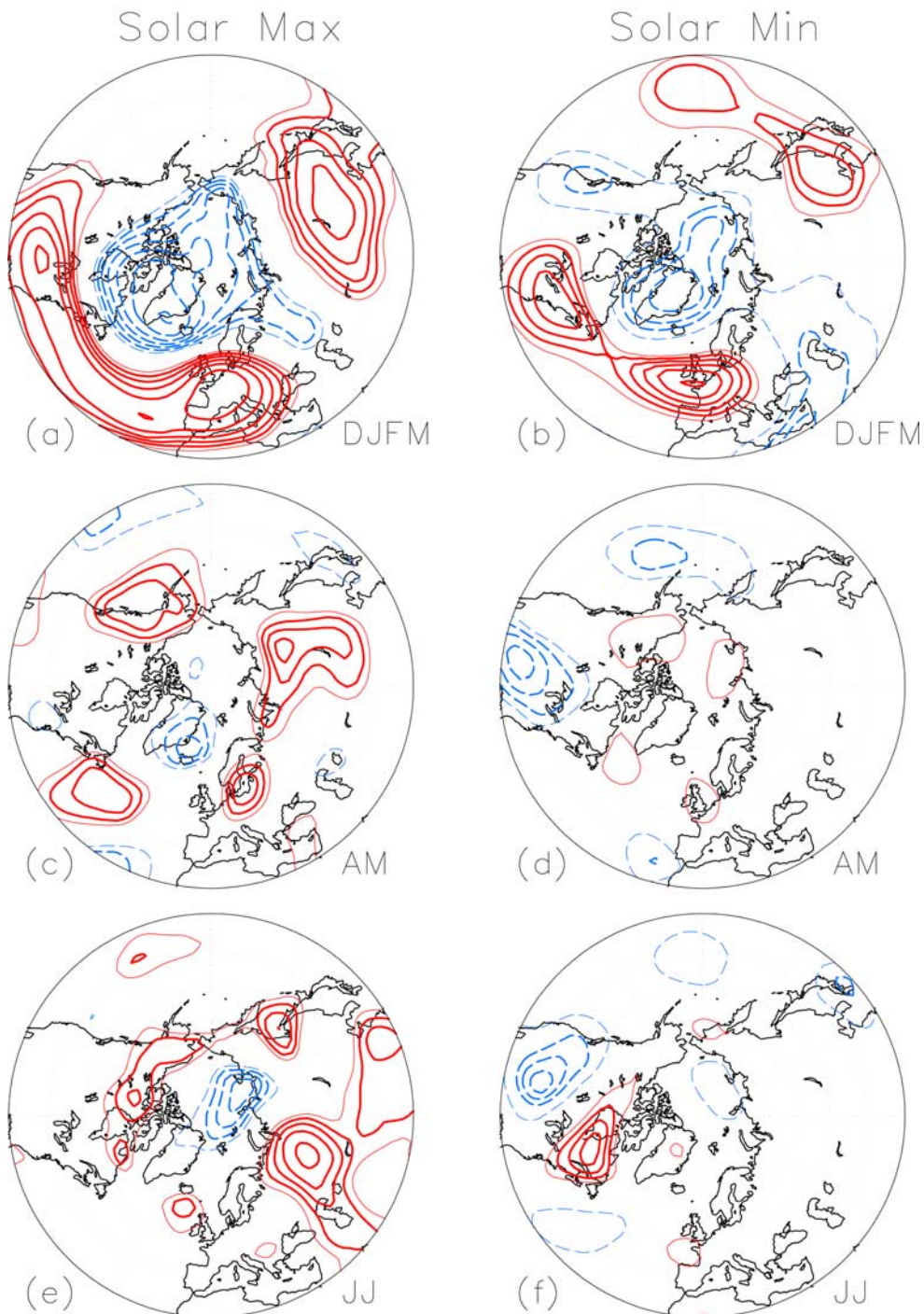


Figure 14. Correlation coefficients of the 500-hPa geopotential height with the winter (December–February) SV NAM index. The 500-hPa geopotential high in (a) the winter (December–March) for the solar max, (b) the winter for the solar min, (c) the spring (April–May) for the solar max, (d) the spring for the solar min, (e) the summer (June–July) for the solar max, and (f) the summer for the solar min. Contours are as in Figure 11.

[33] **Acknowledgments.** We would like to thank anonymous reviewers for their helpful comments and suggestions. The Grid Analysis and Display System (GrADS) was used for drawing figures.

References

- Ambaum, M. H. P., B. J. Hoskins, and D. B. Stephenson (2001), Arctic Oscillation or North Atlantic Oscillation?, *J. Clim.*, *14*, 3495–3507.
- Blackmon, M. L., J. M. Wallace, N.-C. Lau, and S. L. Mullen (1977), An observational study of the Northern Hemisphere wintertime circulation, *J. Atmos. Sci.*, *34*, 1040–1053.
- Hamming, R. W. (1989), *Digital Filters*, 3rd ed., 284 pp., Dover, Mineola, N. Y.
- Hurrell, J. W., and H. van Loon (1997), Decadal variations in climate associated with the North Atlantic Oscillation, *Clim. Change*, *36*, 301–326.
- Hurrell, J. W., Y. Kushnir, G. Ottersen, and M. Visbeck (2003), An overview of the North Atlantic Oscillation, in *The North Atlantic Oscillation*, *Geophys. Monogr. Ser.*, vol. 134, edited by J. W. Hurrell et al., pp. 1–35, AGU, Washington, D. C.
- Itoh, H. (2002), True versus apparent Arctic Oscillation, *Geophys. Res. Lett.*, *29*(8), 1268, doi:10.1029/2001GL013978.
- Kalnay, E., et al. (1996), The NCEP/NCAR 40-year reanalysis project, *Bull. Am. Meteorol. Soc.*, *77*, 437–471.
- Kimoto, M., F.-F. Jin, M. Watanabe, and N. Yasutomi (2001), Zonal-eddy coupling and a neutral mode theory for the Arctic Oscillation, *Geophys. Res. Lett.*, *28*, 737–740.
- Kistler, R., et al. (2001), The NCEP-NCAR 50-year reanalysis: Monthly means CD-ROM and documentation, *Bull. Am. Meteorol. Soc.*, *82*(2), 247–267.
- Kodera, K. (2002), Solar cycle modulation of the North Atlantic Oscillation: Implication in the spatial structure of the NAO, *Geophys. Res. Lett.*, *29*(8), 1218, doi:10.1029/2001GL014557.
- Kodera, K. (2003), Solar influence on the spatial structure of the NAO during the winter 1900–1999, *Geophys. Res. Lett.*, *30*(4), 1175, doi:10.1029/2002GL016584.
- Limpasuvan, V., and D. L. Hartmann (1999), Eddies and the annular modes of climate variability, *Geophys. Res. Lett.*, *26*, 3133–3136.
- Limpasuvan, V., and D. L. Hartmann (2000), Wave-maintained annular modes of climate variability, *J. Clim.*, *13*, 4414–4429.
- Ogi, M., Y. Tachibana, and K. Yamazaki (2003a), Impact of the wintertime North Atlantic Oscillation (NAO) on the summertime atmospheric circulation, *Geophys. Res. Lett.*, *30*(13), 1704, doi:10.1029/2003GL017280.
- Ogi, M., K. Yamazaki, and Y. Tachibana (2003b), Solar cycle modulation of the seasonal linkage of the North Atlantic Oscillation (NAO), *Geophys. Res. Lett.*, *30*(22), 2170, doi:10.1029/2003GL018545.
- Ogi, M., Y. Tachibana, and K. Yamazaki (2004), The connectivity of the winter North Atlantic Oscillation (NAO) and the summer Okhotsk High, *J. Meteorol. Soc. Jpn.*, *82*, 905–913.
- Rogers, J. C. (1997), North Atlantic storm track variability and its association to the North Atlantic Oscillation and climate variability of northern Europe, *J. Clim.*, *10*, 1635–1645.
- Rogers, J. C., and M. J. McHugh (2002), On the separability of the North Atlantic oscillation and Arctic oscillation, *Clim. Dyn.*, *19*, 599–608.
- Serreze, M. C., F. Carse, R. G. Barry, and J. C. Rogers (1997), Icelandic low cyclone activity, climatological features, linkages with the NAO, and relationships with recent changes in the Northern Hemisphere circulation, *J. Clim.*, *10*, 453–464.
- Serreze, M. C., A. H. Lynch, and M. P. Clark (2001), The Arctic frontal zone as seen in the NCEP-NCAR reanalysis, *J. Clim.*, *14*, 1550–1567.
- Thompson, D. W. J., and J. M. Wallace (1998), The Arctic Oscillation signature in the wintertime geopotential height and temperature fields, *Geophys. Res. Lett.*, *25*, 1297–1300.
- Thompson, D. W. J., and J. M. Wallace (2000), Annular modes in the extratropical circulation. part I: Month-to-month variability, *J. Clim.*, *13*, 1000–1016.
- Wallace, J. M. (2000), North Atlantic Oscillation/annular mode: Two paradigms-one phenomenon, *Q. J. R. Meteorol. Soc.*, *126*, 791–805.
- Wallace, J. M., and D. W. J. Thompson (2002), The Pacific center of action of the Northern Hemisphere annular mode: Real or Artifact?, *J. Clim.*, *15*, 1987–1991.
- Yamazaki, K., and Y. Shinya (1999), Analysis of the Arctic Oscillation simulated by AGCM, *J. Meteorol. Soc. Jpn.*, *77*, 1287–1298.

M. Ogi, Frontier Research Center for Global Change, Japan Agency for Marine-Earth Science and Technology, 3173-25 Showa-machi, Kanazawa-ku, Yokohama 236-0001, Japan. (masayo.ogi@jamstec.go.jp)

Y. Tachibana, Liberal Arts Education Center, Tokai University, 1117, Kitakaname, Hiratsuka 2591201, Japan. (tachi@rh.u-tokai.ac.jp)

K. Yamazaki, Graduate School of Environmental Earth Science, Hokkaido University, Kita 8 Nishi 5, Sapporo 060-0808, Japan. (yamazaki@ees.hokudai.ac.jp)